MiR-124 synergism with ELAVL3 enhances target gene expression to promote neuronal maturity

Ya-Lin Lu[a,b,c], Yangjian Liu[a,b], Matthew J. McCoy[a,b,d,1], and Andrew S. Yoo[a,b,2]

[a]Department of Developmental Biology, Washington University School of Medicine, St. Louis, MO 63110; [b]Center for Regenerative Medicine, Washington University School of Medicine, St. Louis, MO 63110; [c]Program in Developmental, Regenerative and Stem Cell Biology, Washington University School of Medicine, St. Louis, MO 63110; and [d]Program in Molecular Genetics and Genomics, Washington University School of Medicine, St. Louis, MO 63110

Edited by Marius Wernig, Stanford University, Stanford, CA, and accepted by Editorial Board Member Brigid L. Hogan April 3, 2021 (received for review July 27, 2020)

Neuron-enriched microRNAs (miRNAs), miR-9/9* and miR-124 (miR-9/9*-124), direct cell fate switching of human fibroblasts to neurons when ectopically expressed by repressing antineurogenic genes. How these miRNAs function after the repression of fibroblast genes for neuronal fate remains unclear. Here, we identified targets of miR-9/9*-124 as reprogramming cells activate the neuronal program and reveal the role of miR-124 that directly promotes the expression of its target genes associated with neuronal development and function. The mode of miR-124 as a positive regulator is determined by the binding of both AGO and a neuron-enriched RNA-binding protein, ELAVL3, to target transcripts. Although existing literature indicates that miRNA–ELAVL family protein interaction can result in either target gene up-regulation or down-regulation in a context-dependent manner, we specifically identified neuronal ELAVL3 as the driver for miR-124 target gene up-regulation in neurons. In primary human neurons, repressing miR-124 and ELAVL3 led to the down-regulation of genes involved in neuronal function and process outgrowth and cellular phenotypes of reduced inward currents and neurite outgrowth. Our results highlight the synergistic role between miR-124 and RNA-binding proteins to promote target gene regulation and neuronal function.

direct reprogramming | neuronal maturity | miR-124 | microRNA target | RNA-binding protein

MicroRNAs (miRNAs) are small noncoding RNAs loaded into Argonuate (AGO) proteins for the formation of the RNA-induced silencing complex (RISC) that functions to repress complementary messenger RNA (mRNA) targets. Brain-enriched miRNAs, miR-9/9* and miR-124 (miR-9/9*-124), function as reprogramming effectors that, when ectopically expressed in human dermal fibroblasts (HDFs), induce an extensive reconfiguration of the chromatin accessibility landscape leading to the erasure of fibroblast fate and activation of the neuronal program (1–3). The conversion process by miR-9/9*-124 shares similarities to molecular cascades underlying neurogenesis during neural development such as the down-regulation of REST, a well-established transcription repressor of neuronal genes (4–6), and switching of homologous chromatin modifiers from nonneuronal to neuronal counterparts including DNMT3B to DNMT3A, subunits of BAF/BRM-associated factor (BAF) complexes, and TOP2A to TOP2B (1, 4, 7–12) due to the repressive activities of the miRNAs. Although the direct repression by brain-enriched miRNAs on nonneuronal targets for initiating the neuronal program (11, 13–15) offer a classic representation of miRNAs acting as negative regulators of target genes, how these miRNAs function within the neuronal gene network remains unknown.

MiR-9/9*-124– or miRNA-induced neurons (miNs) represent a highly enriched population of cells that have reached a neuronal state characterized by the reconfiguration of the chromatin landscape and activation of the general neuronal program, yet lacking maturation into specific neuronal subtypes (1, 2). MiNs are instead poised to take inputs from additional transcription factors to be specified into mature neuronal subtypes. As we noticed the neuronal conversion process was accompanied by cell death (12), we previously modified the miRNA expression vector to include *BCL2L1* (*Bcl-XL*) gene under an inducible promoter to help cells cope with cellular stresses associated with postmitotic reprogramming (16). Expression of *BCL2L1* with a nonspecific miRNA (miR-NS) does not display any reprogramming activity; thus, the conversion mainly comes from miR-9/9*-124 (1, 16). Because early miRNA expression during neuronal conversion functions to repress nonneuronal targets expressed in fibroblasts, we reason that the miRNAs remain necessary for the induction of the neuronal program after the repression of anti-neurogenic genes. In the present study, we performed high-throughput sequencing of RNA isolated by crosslinking immunoprecipitation (HITS-CLIP) of AGO during miR-9/9*-124–mediated neuronal reprogramming of human fibroblasts to map miR-9/9*-124 target interactions at the onset of neuronal fate acquisition. This led to an unexpected identification of neuronal genes enriched with AGO binding, in particular, corresponding to the binding sites of miR-124. The up-regulation of these neuronal genes requires miR-124, suggesting that miR-124 not only functions as a repressor but also as an effector to promote neuronal gene expression. Although the ability of miRNAs as a positive effector of downstream target genes has been implicated before (17–19), little is known about the

Significance

MicroRNAs (miRNAs) are small noncoding RNAs that when loaded into Argonuate (AGO) form the RNA-induced silencing complex that represses target transcripts. Here, in addition to the canonical repressive miRNA function, we identified the activity of miR-124, a neuron-enriched miRNA, as a positive regulator of its target genes. Transcripts harboring both miR-124 and ELAVL3, an RNA-binding protein, target sites at the 3′ untranslated region (3′UTR) allowing for the synergism of AGO-miR124 and ELAVL3 to enhance its target gene expression. The switch of miR-124 as a positive regulator is essential for facilitating neuronal reprogramming of human fibroblasts and promoting the functional maturity of primary human neurons. Our study provides a conceptual advance in microRNA's function in regulating neuronal identity and function.

Author contributions: Y.-L.L., Y.L., and M.J.M. designed research; Y.-L.L., Y.L., and M.J.M. performed research; Y.-L.L., Y.L., and M.J.M. analyzed data; and Y.-L.L. and A.S.Y. wrote the paper.

Competing interest statement: M.W. and M.J.M. are both affiliated with Stanford University.

This article is a PNAS Direct Submission. M.W. is a guest editor invited by the Editorial Board.

[1]Present address: Department of Pathology, Stanford University School of Medicine, Stanford, CA 94305.

[2]To whom correspondence may be addressed. Email: yooa@wustl.edu.

This article contains supporting information online at https://www.pnas.org/lookup/suppl/doi:10.1073/pnas.2015454118/-/DCSupplemental.

Published May 24, 2021.

molecular mechanism that governs a miRNA's activity as a positive regulator of target genes in neurons and the identity of activated target genes. Here, we use homologous genes, *PTBP1* and *PTBP2*, as a model to dissect how miR-124 selectively up-regulates PTBP2 expression in neurons and reveal genetic networks that are enhanced by miR-124 in both reprogrammed and primary human neurons (HNs).

Results

AGO Binds Both Down-Regulated and Up-Regulated Genes during miR-9/9*-124–Mediated Direct Neuronal Reprogramming of Human Fibroblasts. Previous studies showed that the ectopic expression of miR-9/9*-124 in HDFs induces a neuronal state characterized by the appearance of neuronal markers (such as MAP2, TUBB3, NCAM, and SNAP25) (Fig. 1*A* and *SI Appendix*, Fig. S1) and electrical excitability (1, 2). To identify target genes of miR-9/9*-124 as reprogramming cells transition to neuronal identity, we carried out AGO HITS-CLIP by sequencing bound transcripts upon AGO immunoprecipitation after 2 wk into reprogramming, a time point when neuronal genes are activated (1, 2). The goal was to identify transcripts bound by AGO loaded with miR-9/9* or miR-124 over the miR-NS control ($Log_2FC \geq 1$, adj.*P* value < 0.05). We compared these hits to the list of differentially expressed genes (DEGs) (by RNA sequencing [RNA-seq] analysis; $-1 \geq Log_2FC \geq 1$, adj.*P* value < 0.05) at day 20 of miNs (1). As expected, we found target transcripts that were down-regulated, consistent with the repressive mode of miRNAs (Fig. 1*B*, 113 genes labeled as green dots) including some known targets, *SHROOM3* and *PHF19* (20–22). Interestingly, we also discovered 453 unique gene transcripts with enriched AGO binding, which were up-regulated in day 20 mins (Fig. 1*B*, red dots). By gene ontology (GO) analysis, these up-regulated genes with enriched AGO binding in response to miR-9/9*-124 were associated with various neuronal processes such as synaptic transmission and regulation of membrane potential (red), in contrast to nonneuronal, down-regulated target genes (green) (Fig. 1*C*). Several of these identified AGO HITS-CLIP targets can also be independently validated in additional reprogramming lines through RNA-binding protein (RBP) immunoprecipitation (RIP) of AGO followed by qRT-PCR (*SI Appendix*, Fig. S1). Moreover, when examined against the time course transcriptome analysis during neuronal reprogramming (1), the identified neuronal target genes showed continuous up-regulation during later time point of neuronal conversion (Fig. 1*D*). For example, neuronal transcripts such as *MAP2*, *PTBP2*, and *SLC4A8* that were highly expressed in day 20 mins also harbored AGO binding sites at the 3′ untranslated region (3′UTR) (Fig. 1*E*). To determine the fraction of up-regulated neuronal genes that are likely actual targets of miR-9/9* and/or miR-124, we extracted the miRNA-bound or AGO-enriched sequences and predicted the duplex formation by either miR-9/9* and/or miR-124 through RNAhybrid (a maximum free energy threshold of −20 kcal/mol) (23). Of the 453 up-regulated DEGs in miNs bound by AGO (Fig. 1*B*), 328 (~72%) gene transcripts are predicted to contain miR-9/9* and/or miR-124 binding sites (Fig. 1*F*). These transcripts harboring miR-9/9*-124 sites are also associated with the similar set of neuronal GO terms in Fig. 1*C* as they include a selection of genes important for neuronal function (Fig. 1*F*). Of these up-regulated miR-9/9*-124 target genes, more than 94% of the total genes (308 of 328 genes) contain miR-124 target sequence alone (45%) or with miR-9/9* sites, while less than 6% of the genes (20 genes) contain miR-9/9* target sites only (Fig. 1*G*). These results collectively demonstrate that the AGO-loaded transcripts differentially (up or down) respond to miR-9/9*-124 during neuronal conversion.

MiR-124 Target Genes Are Up-Regulated during Neuronal Conversion. As a large fraction of the up-regulated genes contained miR-124 target sequences (Fig. 1*G*), we further tested whether the up-regulated genes were bona fide targets of miR-124 by knocking down miR-124 expression through the use of a tough decoy (TuD) to inhibit miRNA activity (24, 25). The effect of the lentivirus-based TuD for miR-124 (TuD-miR-124) was monitored after transduction by following the concurrent expression of TurboRFP reporter and measuring the mature miR-124 level. Knockdown (KD) of miR-124 yielded more than 60% reduction of miR-124 expression in comparison to the control, miR-NS TuD (TuD-miR-NS) (*SI Appendix*, Fig. S2 *A* and *B*). We then performed RNA-seq analysis on day 21 mins treated with either control or miR-124 TuD to see whether any of the miR-124 target would fail to be up-regulated upon reduced miR-124 activity (Fig. 2*A* and *SI Appendix*, Fig. S2*C*). When compared with up-regulated DEGs in day 20 mins that were also enriched for AGO binding (Fig. 1), we identified 192 genes ($Log_2FC \leq 0.5$, adj.*P* value < 0.01) that failed to be up-regulated upon miR-124 reduction (Fig. 2*A* and *SI Appendix*, Table S1). We further validated by qPCR a select number of these targets when miR-124 was knocked down at day 14 into conversion, an earlier time point when neuronal genes are emerging (*SI Appendix*, Fig. S2 *D* and *E*) (1, 2). Furthermore, the effect of TuD was further corroborated by independent methods using CRISPR-based KD approaches (*SI Appendix*, Fig. S3) (26). With GO analysis, these identified genes were associated with neuronal terms involved in various synaptic processes (Fig. 2*B*).

To further analyze miR-124 target interactions, we looked into the potential duplex formations between miR-124 and the identified AGO HITS-CLIP peak regions using RNAhybrid (a maximum free energy threshold of −20 kcal/mol) (23). Of the up-regulated transcripts that harbor AGO-enriched peaks, we identified a spectrum of miR-124 and target mRNA duplex configurations ranging from the canonical two- to eight-seed base pairing to noncanonical base pairing starting at position 3 and 4 (Fig. 2*C* and *SI Appendix*, Figs. S2*F* and S4). These examples include *MAP2* 3′UTR, in which miR-124 base pairing is predicted to start at position 3, while miR-124 target sequences on *PTBP2* 3′UTR at the two peaks are predicted to start at position 1 and position 2, respectively (Fig. 2*C*). Interestingly, across the predicted miR-124:target duplex configurations, we observed consistent auxiliary 2 to 3 base pairing at the 3′ end of miR-124 (*SI Appendix*, Fig. S2*F*).

Our results so far indicate that miR-124 can target and promote the expression of select neuronal genes as cells acquire the neuronal fate during conversion. Subsequently, we questioned whether the active mode of miR-124 would be specific to neuronal cell types. We cloned the 3′UTRs of several identified, up-regulated targets (*MAP2*, *PTBP2*, *BCL7A*, *KALRN*, *SEMA6A*, and *RCAN2*) into a luciferase reporter for transfection into a nonneuronal cell type, HEK293T (a human embryonic kidney cell line), with a miR-9/9*-124 expression construct. After 48 h, we found that unlike reprogrammed neurons, miR-9/9*-124 can bind and repress the 3′UTRs of neuronal genes as indicated by the reduced luciferase activity in HEK293T cells, while the nontarget control *PGK1* 3′UTR was unaffected (Fig. 2*D*). This result suggests that additional determinants available in neuronal cells that are otherwise absent in nonneuronal cells may govern the activity of miR-124 as a positive regulator while simultaneously functioning to repress nonneuronal targets (Fig. 2*E*).

PTBP1 and PTBP2 3′UTR as Targets of miR-124. To dissect the mechanism underlying the dual modes of miR-124 on its targets, we elected to focus on *PTBP2* from the list of our identified neuronal targets because 1) *PTBP2* and its nonneuronal homolog, *PTBP1*, both contain miR-124 sites in their 3′UTRs (Fig. 3*A*), and 2) both *PTBP1* and *PTBP2* 3′UTRs are targeted and repressed by miR-124 in HEK293T cells (Fig. 3*A*), but 3) contrastingly, as observed in the human brain, qPCR analysis showed that the neuronal conversion established the mutually exclusive expression between *PTBP1* and *PTBP2* (Fig. 3*B*). Therefore, the PTB homologs

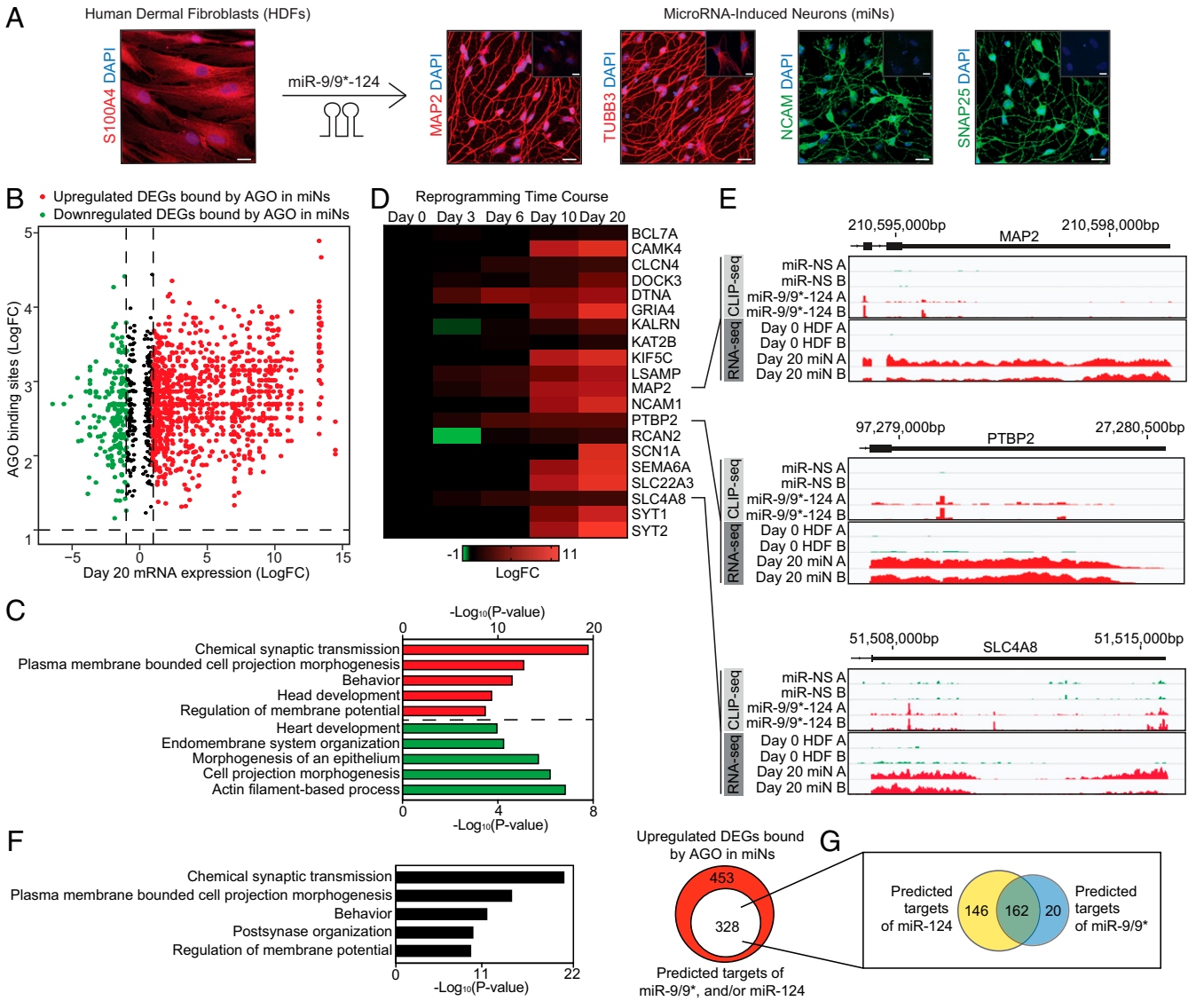

Fig. 1. Enrichment of AGO binding on transcripts of neuronal genes up-regulated during miR-9/9*-124–mediated neuronal conversion. (*A*) Examples of miR-9/9*-124–mediated direct reprogramming of HDFs into miNs. Images show immunostaining of the fibroblast marker (S100A4) and neuronal markers (MAP2, TUBB3, NCAM, and SNAP25). The insets represent staining of HDFs treated with miR-NS. (Scale bar, 20 μm.) (*B*) A volcano plot of DEGs at day 20 miNs and enrichment of AGO binding in response to miR-9/9*-124 expression identified by AGO HITS-CLIP analysis. Red dots, day 20 mRNA expression; Log2FC ≥ 1, adj.*P* value < 0.05; AGO binding Log2FC ≥ 1, adj.*P* value < 0.05. Green dots, day 20 mRNA expression; Log2FC ≤ -1, adj.*P* value < 0.05; AGO binding Log2FC ≥ 1, adj.*P* value < 0.05. (*C*) Top biological GO terms of up-regulated (red) and down-regulated (green) DEGs in day 20 miNs differentially bound by AGO. (*D*) Time course heatmap of select up-regulated DEGs enriched for AGO binding with miR-9/9*-124 expression. (*E*) Track views of AGO HITS-CLIP (*Top*) and RNA-seq (*Bottom*) of genes with 3′UTR showing the enrichment of AGO binding in miR-9/9*-124 condition (over control miR-NS) and increased transcript levels. (*F*) Of the 453 unique up-regulated DEGs identified in *B*, 328 are predicted to harbor miR-9/9* and/or miR-124 sites at the AGO-enriched regions through RNAhybrid prediction. The graph indicates top biological GO terms associated with the 328 up-regulated DEGs containing miR-9/9* and/or miR-124 target sites. (*G*) Breakdown of the 328 up-regulated DEGs in *F* based on common or specific targets of miR-9/9* and/or miR-124.

represent an ideal example to investigate how two closely related targets respond differently to miR-124.

The 3′UTRs of human *PTBP1* and *PTBP2* contain two predicted target sites for miR-124 (yellow bar) and one site for miR-9 (blue bar) (Fig. 3*A*). Luciferase reporter assays in nonneuronal HEK293T cells showed that miR-9/9*-124 or miR-124 alone (but not miR-9/9* alone) repressed both *PTBP1* and *PTBP2* through their 3′UTRs indicating that miR-124 is the primary miRNA targeting both PTB 3′UTRs (Fig. 3*A*). Mutating the two miR-124 sites in *PTBP2* 3′UTR (s1 and s2) rendered the 3′UTR insensitive to miR-124 (*SI Appendix*, Fig. S5*A*). While our results pointing to the ability of miR-124 to target and repress 3′UTRs of both *PTBP1* and *PTBP2* in cell lines were consistent with previous findings (13, 27), it remains unknown how miRNA-mediated neuronal conversion of fibroblasts establishes the mutually exclusive expression of PTBP1 and PTBP2 as seen in the human brain (Fig. 3*B*) and in in vivo neurons (28).

Because *PTBP1* and *PTBP2* are regulated differentially in miNs, we asked whether the repressive activity of miR-124 on *PTBP2* 3′UTR could be reversed with a prolonged neurogenic input by miR-9/9*-124 in HEK293T cells. We expressed a destabilized EGFP reporter containing *PTBP1* 3′UTR, *PTBP2* 3′UTR, or CTL that lacks a 3′UTR in HEK293T cells with the miR-9/9*-124 expression construct (*SI Appendix*, Fig. S5*B*). Analogous to PTBP2 up-regulation during neuronal reprogramming of HDFs, we observed the selective repression of EGFP with *PTBP1* 3′UTR but not

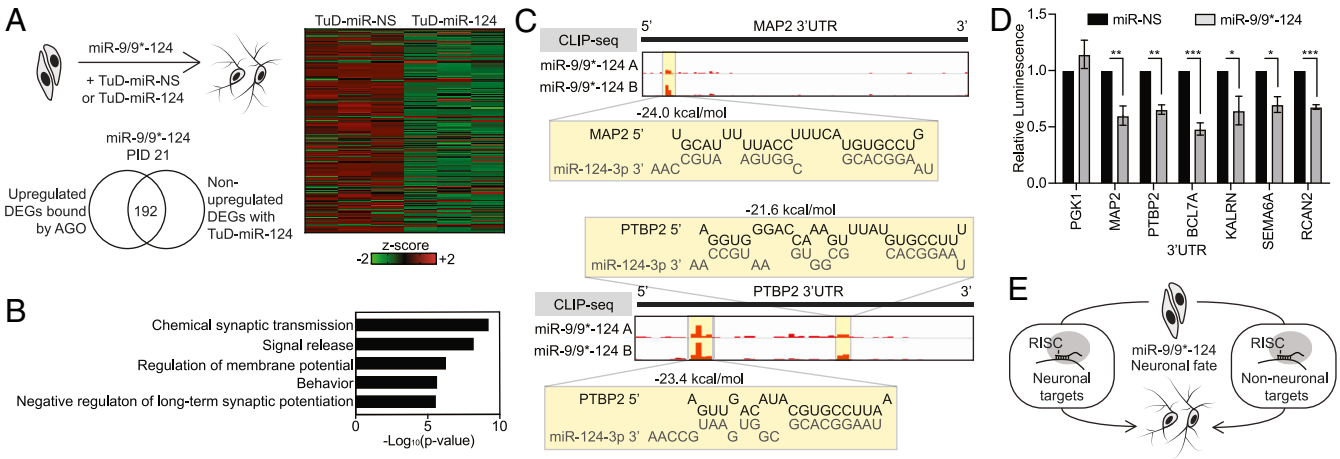

Fig. 2. Identification of miR-124 target genes that fail to be up-regulated upon the inhibition of miR-124 during miRNA-mediated neuronal conversion. (*A*) *Left*, miR-124 activity is reduced through the use of TuD. By overlapping with up-regulated DEGs bound by AGO (Fig. 1), 192 genes were identified as genes that fail to be up-regulated upon reduced miR-124 activity. (*Right*) A heatmap of the 192 genes from RNA-seq comparing miNs treated with TuD against miR-NS (TuD-miR-NS) or miR-124 (TuD-miR-124). (*B*) Top biological GO terms associated with the 192 genes identified in *A*. (*C*) Predicted binding of miR-124 to the 3′UTR sequences of neuronal target genes with MAP2 and PTBP2 as examples, according to RNAhybrid prediction at the highlighted AGO HITS-CLIP peaks. (*D*) Luciferase assays in HEK293T cells of up-regulated neuronal target genes of miR-124 selected from *A*. In nonneuronal context of HEK293T cells, 3′UTRs of the identified neuronal genes can be targeted and repressed by miR-9/9*-124. Luminescence was measured after 48 h of transfection and normalized to miR-NS control of each condition. Data are represented by mean ± SEM from three independent experiments. Two-tailed unpaired *t* test (from left, $^{**}P = 0.0094$, $P = 0.0011$; $^{***}P < 0.001$; $^{*}P = 0.048$, $P = 0.012$; $^{***}P < 0.001$). (*E*) A diagram of the observed phenomenon in which miR-9/9*-124 can promote neuronal identity by simultaneously targeting both nonneuronal genes for repression while promoting the expression of neuronal genes during neuronal conversion.

PTBP2 3′UTR (*SI Appendix*, Fig. S5 *B* and *C*). These results suggest that with prolonged neurogenic input, *PTBP2* 3′UTR responds to miR-124 differentially from when measured after 48 h with miRNA expression in HEK293T cells (Figs. 2*D* and 3*A*).

MiR-124 Accentuates PTBP2 Expression beyond the Induction Mediated by the Down-Regulation of PTBP1. Previous studies have shown that during development, PTBP1 destabilizes *PTBP2* transcript in non-neuronal cells by alternative splicing, and at the onset of neurogenesis, miR-124 directly represses *PTBP1* resulting in PTBP2 induction (13, 28). Upon miR-9/9*-124 expression in HDFs, we observed the concomitant down-regulation and up-regulation of endogenous PTBP1 and PTBP2, respectively (Fig. 3*B*). As expected, the initial PTBP2 up-regulation was abrogated when *PTBP1* complementary DNA (cDNA) was overexpressed (Fig. 3*C*), supporting the role of PTBP1 reduction as the initiation step of PTBP2 expression. We then sought to stratify the contribution of PTBP1 repression alone versus the input of miRNAs to the overall PTBP2 level. When PTBP2 protein levels were compared between PTBP1 KD with a short hairpin RNA (shRNA) and miR-9/9*-124 expression, we found that miR-9/9*-124 enhanced PTBP2 level by approximately twofold over the PTBP1 KD-alone condition (Fig. 3*D*). In fact, PTBP2 was more up-regulated with miR-9/9*-124 despite a more pronounced reduction of PTBP1 with shRNA (Fig. 3*D*), demonstrating that miR-9/9*-124 accentuate PTBP2 expression beyond the level induced by PTBP1 down-regulation.

Functional Significance of PTBP2 Up-Regulation for Neuronal Conversion. To probe the functional importance of *PTBP2* expression, we knocked down *PTBP2* with shRNA during neuronal conversion. *PTBP2* shRNA completely impaired the induction of neurons marked by the loss of MAP2 expression, a neuronal marker (Fig. 3*E*). The effect of shRNA was specific to *PTBP2* KD as supplementing *PTBP2* cDNA rescued the reprogramming defect (Fig. 3*E*). These findings were somewhat surprising as the results from a previous study indicated that sequential reduction of PTBP2 by shRNA was found to promote maturation of reprogrammed neurons (27); however, our results indicate that at least at the initiation of reprogramming, PTBP2 is critical. While it is not clear why shRNA- versus miRNA-based reprogramming approaches lead to these different results, our results demonstrate the essential role of PTBP2, at least, at the onset of neuronal conversion. Furthermore, knocking down PTBP2 in primary cultured HNs resulted in increased cell death as measured with SYTOX assay (*SI Appendix*, Fig. S6 *A* and *B*), consistent with previous studies that showed the essential function of PTBP2 in primary neurons (29).

We also performed Human Clariom D Assay in HDFs expressing the nonspecific control miR-NS, miR-9/9*-124, or miR-9/9*-124 with *PTBP2* shRNA to identify genes whose expression and alternative splicing patterns were affected by the reduction of PTBP2. By 2 wk, miR-9/9*-124–expressing cells showed significant down-regulation of *PTBP1* and other fibroblast-enriched genes such as *FBN1* and *S100A4* and up-regulation of *PTBP2* and neuronal genes (for example, *NEFM* and *SNAP25*) in comparison to the control miR-NS (FC ≥ 1.5, ANOVA *P* value < 0.05) (*SI Appendix*, Fig. S6*C*) (1). Alternative splicing events mediated by PTBP2 were examined by comparing spliced events between *PTBP2* shRNA and control shRNA (shCTL) conditions. We found that reducing PTBP2 led to changes in splicing events ($-2 \geq$ splicing index ≥ 2, ANOVA *P* value < 0.05) indicated by red (positive splicing index) and green dots (negative splicing index) (*SI Appendix*, Fig. S6*D*). This analysis identified known splicing targets of PTBP2, such as the exon skipping or exclusion in *UNC13B*, *DLG4*, and *CADM3* and inclusion in *DNM1* and *SMARCC2* transcripts (*SI Appendix*, Fig. S6*D*) (29–32). Comparing genes up-regulated in response to miR-9/9*-124 to genes associated with PTBP2-mediated alternative splicing (differential splicing events between miR-9/9*-124-shCTL and shPTBP2 conditions) identified 1,183 differentially spliced transcripts of genes involved in processes such as neuronal differentiation and signaling (*SI Appendix*, Fig. S6*E*) (*SI Appendix*, Table S2). Altogether, our results support the role of PTBP2 as a crucial regulator of the neuronal program.

Differential Sequence Composition between PTBP1 and PTBP2 3′UTRs. Using PTBP1 down-regulation and PTBP2 up-regulation as a model, we sought to identify effectors that determine miR-124

function as a positive regulator (Fig. 3*F*). RBPs including PTB proteins have been studied for their diverse roles in posttranscriptional regulation of mRNAs not limited to alternative splicing and transcript stability (33). In addition, RBPs have been shown to interact with miRNA-loaded RISC complexes to modulate target gene expression (34–36). We ran the sequence of *PTBP2* 3′UTR through three RBP motif prediction databases, including RBPDB (37), RBPmap (38), and beRBP (39) (*SI Appendix*, Fig. S7*A*). Across the three databases, two RBPs, ELAVL1 and PUM2, were consistently predicted to bind to *PTBP2* 3′UTR (*SI Appendix*, Fig. S7*A*). As PTBP2 up-regulation occurs in neurons, we focused on the family of RBPs whose expression is neuronally enriched. Whereas *ELAVL1* and Pumilio family members, *PUM2* and *PUM1*, are ubiquitously expressed (40–42), other ELAVL family members, *ELAVL2*, *ELAVL3*, and *ELAVL4* (collectively referred to as neuronal *ELAVLs* and *nELAVLs*), have been shown to be neuronally enriched (42). We also examined the HITS-CLIP data of nELAVLs in the human brain (43) and found nELAVLs to be highly enriched at *PTBP2* 3′UTR, in contrast to *PTBP1* 3′UTR (*SI Appendix*, Fig. S7 *B* and *C*). Interestingly, *PTBP2* 3′UTR contains AU-rich elements (AREs) that ELAVLs have been shown to bind to (43, 44), in contrast to *PTBP1* 3′UTR that lacks AU-rich sequences (*SI Appendix*, Fig. S7 *B* and *C*). Moreover, nELAVL binding mapped to the AREs around the first miR-124 site (s1; seed, highlighted in red) *PTBP2* 3′UTR (*SI Appendix*, Fig. S7*C*). We thus examined by qPCR whether nELAVLs are induced during neuronal conversion as well as other brain-enriched NOVA-, RBFOX-family proteins, and SSRM4. We found selective up-regulation of nELAVLs with other neuronal RBPs in miNs similarly to the human brain, in contrast to the ubiquitous expression of *ELAVL1* (Fig. 4*A*) (42). To determine whether nELAVL induction occurs concurrently with PTBP2 up-regulation, we assessed ELAVL expression at multiple time points of neuronal conversion. We found that the transcriptional activation of nELAVLs, with *ELAVL3* being the most robust one (blue), aligned with the up-regulation of *PTBP2* (black) by nine days into reprogramming (Fig. 4*B*).

MiRNA-Mediated PTBP2 Induction Requires ELAVL3 Binding at PTBP2 3′UTR. We then tested whether AREs within *PTBP2* 3′UTR would serve as a sequence that binds ELAVL proteins. We expressed 3′UTRs of *PTBP1*, *PTBP2,* or *PTBP2* without the ARE (*PTBP2ΔARE* 3′UTR) along with individual FLAG-tagged ELAVLs (ELAVL1-4) in HEK293T cells (Fig. 4*C*). RNA-immunoprecipitation (RIP) of tagged ELAVLs, followed by qPCR for detecting the bound PTB 3′UTRs, displayed significant enrichment for *PTBP2* 3′UTR with nELAVL (ELAVL2, 3, and 4) pull-downs, while the binding of nonneuronal ELAVL1 to *PTBP2* 3′UTR was minimal. We could not detect significant enrichment for *PTBP1* 3′UTR for any of the ELAVLs (Fig. 4*C*). Importantly, deleting the ARE in *PTBP2* 3′UTR (*PTBP2ΔARE* 3′UTR) abolished the binding of nELAVLs to *PTBP2* 3′UTR (Fig. 4*C*), indicating that such an element within *PTBP2* 3′UTR serves to recruit nELAVLs.

We then asked whether adding nELAVLs to the nonneuronal context of HEK293T cells, thereby reconstituting nELAVLs that become available during neuronal conversion, would alleviate miR-124–mediated repression of PTBP2 and enhance PTBP2 expression. Adding individual ELAVLs to control *PGK1* 3′UTR had no effect on luminescence (relative luminescence of ∼1; *PGK1* 3′UTR histograms) (Fig. 4*D*). Luciferase activities with *PTBP1* 3′UTR remained repressed upon miR-9/9*-124 expression compared to the control miR-NS irrespective of ELAVL addition (relative luminescence of < 1; *PTBP1* 3′UTR histograms) (Fig. 4*D*). MiR-9/9*-124 led to the repression *PTBP2* 3′UTR in the absence of ELAVLs (black, relative luminescence ratio < 1; *PTBP2* 3′UTR histograms) (Fig. 4*D*). However, adding ELAVL2 (green) and ELAVL3 (blue) significantly alleviated miR-9/9*-124–mediated repression on *PTBP2* 3′UTR, with ELAVL3 (blue) having the most significant effect (Fig. 4*D*). To examine the requirement of AREs for ELAVL binding, we repeated the experiments using the *PTBP2* 3′UTR lacking the AU-rich sequence (*PTBP2ΔARE*). Deleting this AU-rich region abolished the effect of ELAVL3 (blue) on *PTBP2* (*PTBP2ΔARE* 3′UTR histograms), which remained repressed (Fig. 4*D*), demonstrating the requirement of ELAVL3 and the ARE for *PTBP2* up-regulation by miR-124.

Selective Activity of ELAVL3 on PTBP2 3′UTR Is Dependent on the Hinge Region. ELAVL1 through 4 members exhibit high sequence homology across all three functional RNA recognition motifs (RRMs) except for the nonconserved spacer region (also referred to as hinge region) flanked by RRM2 and RRM3 (42, 45). To better understand the specificity of ELAVL3 on *PTBP2* 3′UTR regulation, we mutagenized the hinge region of *ELAVL1* and *ELAVL3* by deleting or swapping the hinge region between *ELAVL1* and *ELAVL3*. Deleting the hinge in *ELAVL3* (*ELAVL3ΔH*) (light blue) abrogated the alleviating effect on *PTBP2* 3′UTR repression, whereas no effect was observed with control *PGK1* 3′UTR (Fig. 4*E*, *PGK1* 3′UTR histograms). Moreover, replacing the *ELAVL3* hinge with that of *ELAVL1*'s (*ELAVL3-E1H*) (dark blue) led to the failure of alleviating the *PTBP2* 3′UTR repression (Fig. 4*E*), and none of the *ELAVL3* variants (wild-type and mutants) had any effect on *PTBP2* 3′UTR lacking the AU-rich region (Fig. 4*E*, *PTBP2ΔARE* 3′UTR histograms). These results indicate that the specificity of ELAVL3 to *PTBP2* 3′UTR is mediated by the *ELAVL3* hinge region. This notion is further supported by the increase in the luminescence readout of *PTBP2* 3′UTR in HEK293T cells when *ELAVL1* hinge is replaced by *ELAVL3* hinge (*ELAVL1-E3H*) (dark red) compared to wild-type *ELAVL1* (red) (Fig. 4*F*, *PTBP2* 3′UTR histograms).

ELAVL3 Promotes PTBP2 Expression during Neuronal Reprogramming. To further examine whether ELAVL3 would be critical for PTBP2 up-regulation during the neuronal conversion of HDFs, we knocked down *ELAVL3* by shRNA (shELAVL3) to assess PTBP2 expression and neuronal reprogramming. Knocking down ELAVL3 resulted in the significant down-regulation of PTBP2 expression as determined by immunostaining, qPCR, and immunoblotting analyses and impairment of the conversion process (Fig. 5 *A*–*C* and *SI Appendix*, Fig. S7*D*). This KD effect was specific for ELAVL3 down-regulation as PTBP2 expression and neuronal fate acquisition could be rescued with *ELAVL3* cDNA in the presence of shELAVL3 (Fig. 5*A*). It is noteworthy that reducing the function of other nELAVLs (ELAVL2 and 4) had a milder effect on PTBP2 expression (Fig. 5 *B* and *C* and *SI Appendix*, Fig. S7*D*), highlighting the role of ELAVL3 as a primary driver for PTBP2 up-regulation with miR-124.

Synergism between nELAVL and AGO Requires miR-124 Site in PTBP2 3′UTR. We further tested whether the miR-124 sites within *PTBP2* 3′UTR would also be critical for mediating the PTBP2 up-regulation with ELAVL3. By mutating the two miR-124 seed-match sites within *PTBP2* 3′UTR (*PTBP2Δs1s2* 3′UTR), adding any ELAVL failed to enhance the luciferase activity over the control (CTL, black; relative luminescence ratio unchanged; *PTBP2Δs1s2* 3′ UTR histograms) (Fig. 5*D*). This result is in contrast to wild-type *PTBP2* 3′UTR in which ELAVL3 can enhance luciferase activity in the presence of miR-124 target sites (Figs. 4*D* and 5*D*). Interestingly, the lack of increased luminescence with ELAVL3 addition was not due to the failure of ELAVL binding to mutated *PTBP2Δs1s2* 3′UTR because qPCR analysis followed by ELAVL pulldown showed persistent binding of nELAVLs to *PTBP2Δs1s2* 3′UTR (Fig. 5*E*). These results altogether suggest the requirement of both AREs and miR-124 sites in *PTBP2* 3′UTR for PTBP2 up-regulation (Fig. 5*F*).

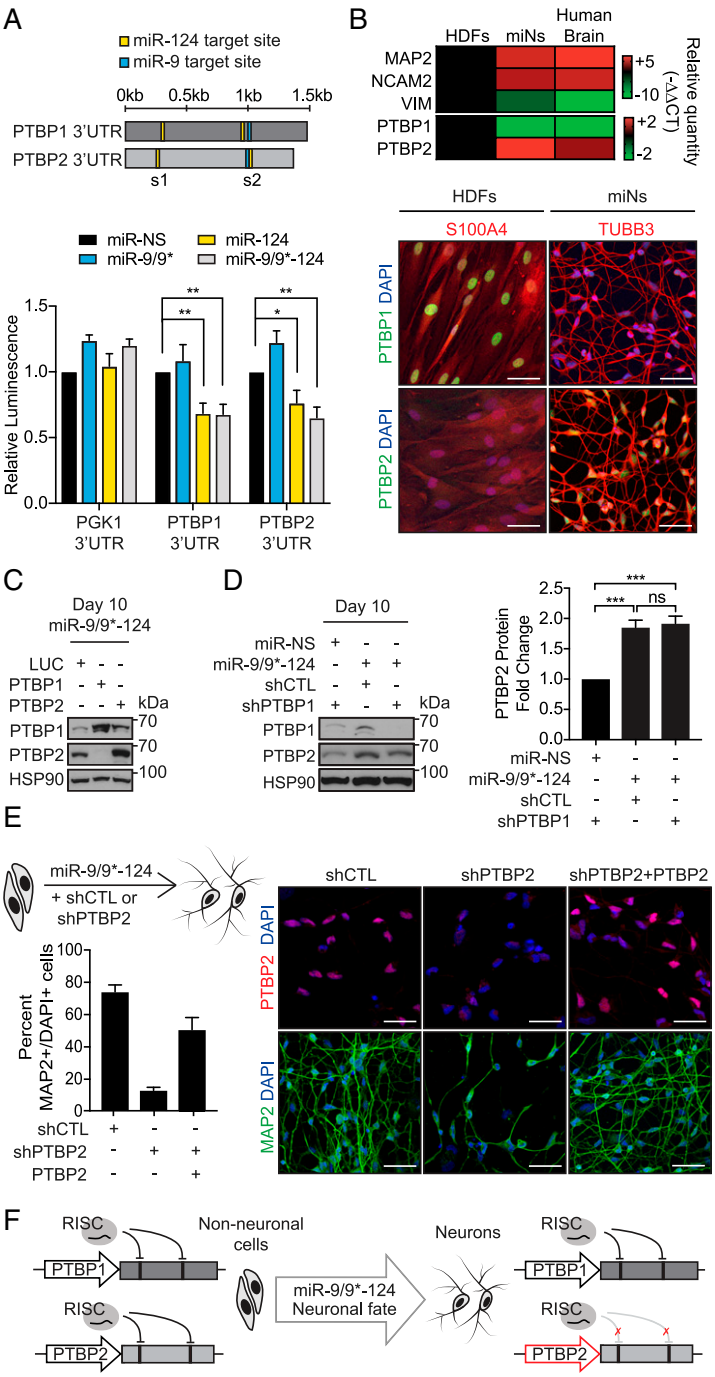

Fig. 3. MiR-124 targets both PTBs but differentially regulates PTB expression during neuronal conversion. (*A*) (*Top*) A schematic diagram of PTB 3′UTRs with miR-124 (yellow) and miR-9 (blue) target sites. s1 and s2 refer to the two conserved miR-124 target sites on PTBP2 3′UTR. (*Bottom*) Luciferase assays with luminescence measured after 48 h of transfection and normalized to miR-NS control in each condition. Data are represented by mean ± SEM from four independent experiments. Two-way ANOVA was performed (from left, PTBP1 3′UTR $^{**}P = 0.0043$, 0.0034; PTBP2 3′UTR $^{*}P = 0.0355$, $^{**}P = 0.0016$). (*B*) (*Top*) A heatmap of gene expression assessed by qPCR in starting HDFs, day 30 miNs, and human brain RNA. Data from HDFs and day 30 miNs are from three independent experiments. (*Bottom*) PTB switching is recapitulated during the miRNA-mediated direct conversion of HDFs into neurons. HDFs and day 30 miNs immunostained for PTBP1 and PTBP2 along with a fibroblast marker, S100A4, and a pan-neuronal marker, TUBB3. (Scale bar, 50 μm.) (*C*) Initial induction of PTBP2 by the reduction of PTBP1 by either shRNA or miRNAs during miRNA-mediated neuronal reprogramming. PTBP1 overexpression in miR-9/9*-124 expression background suppresses PTBP2 induction. (*D*) (*Left*) An immunoblot showing PTBP1 KD in HDFs resulted in induction of PTBP2, but PTBP2 expression becomes more pronounced in the presence of miR-9/9*-124 compared to PTBP1 KD only. (*Right*) Quantification of PTBP2 band intensity as relative fold change compared to PTBP1 KD alone. Data were normalized to HSP90 from four independent experiments. The plots were represented in mean ± SEM. One-way ANOVA was performed (from top $^{***}P = 0.0002$, 0.0004; not significant [ns] $P = 0.8925$). (*E*) (*Top*, *Left*) A schematic diagram of the experimental procedure. (*Right*) Images of day 30 miNs treated with CTL shRNA, PTBP2 shRNA, or PTBP2 shRNA with PTBP2 cDNA. Cells were immunostained for PTBP2 and MAP2. (*Bottom*, *Left*) Quantification of the percentage of MAP2-positive cells with two or more neurite processes over the total number of DAPI-positive cells. (Scale bar, 50 μm.) Data are represented as mean ± SEM. One-way ANOVA was performed ($^{***}P < 0.0001$; ** P 0.0016). shCTL, n = MAP2 356/482; shPTBP2, n = MAP2 31/239; shPTBP2+PTBP2, n = MAP2 225/454. (*F*) A model of differential miR-124 activity on PTB 3′UTRs during neuronal conversion.

Neuronal Genes Down-Regulated upon Loss of miR-124 and ELAVL3 in Human Neurons. To test whether the synergism of miR-124 and ELAVL3 for miRNA-mediated up-regulation is unique to PTBP2 or a broader mechanism applicable to other genes beyond reprogrammed neurons, we performed loss-of-function studies on primary HNs (HNs). With the same TuD for miR-124 (TuD-miR-124) and shELAVL3 constructs used in reprogrammed neurons, miR-124 and ELAVL3 were knocked down in HNs and processed for RNA-seq (Fig. 6 *A* and *B* and *SI Appendix*, Fig. S8*A*). To identify potential targets up-regulated by miR-124 and ELAVL3 in HNs, we focused on genes suppressed upon miR-124 and ELAVL3 loss-of-function (KD, $\text{Log}_2\text{FC} \leq -1$; adj.$P$ value < 0.05) compared to CTL (Fig. 6*B*). Many of these down-regulated genes are neuronal related, including *MAP2*, *PTBP2*, *SCN1A*, and *SEMA6A* (Fig. 6*B*). Despite the down-regulation of several neuronal transcripts, overall neuronal identity remains intact as expression of neuronal markers such as *RBFOX2*, *FMR1*, and *NEFL* remain similar between CTL and KD HNs (*SI Appendix*, Fig. S8*B*). Furthermore, we also do not observe an emergence of progenitor marker expression upon KD of both miR-124 and ELAVL3 (*SI Appendix*, Fig. S8*B*).

To ensure that these down-regulated genes are miR-124 targets, we compared the down-regulated DEGs from HNs to up-regulated DEGs in day 20 mins that also harbor AGO-enriched peaks (Fig. 1). This comparison resulted in a set of 132 target genes associated with biological GO terms related to neuronal development and projection (Fig. 6*C* and *SI Appendix*, Table S3), further validating miR-124 as a positive regulator of the neuronal

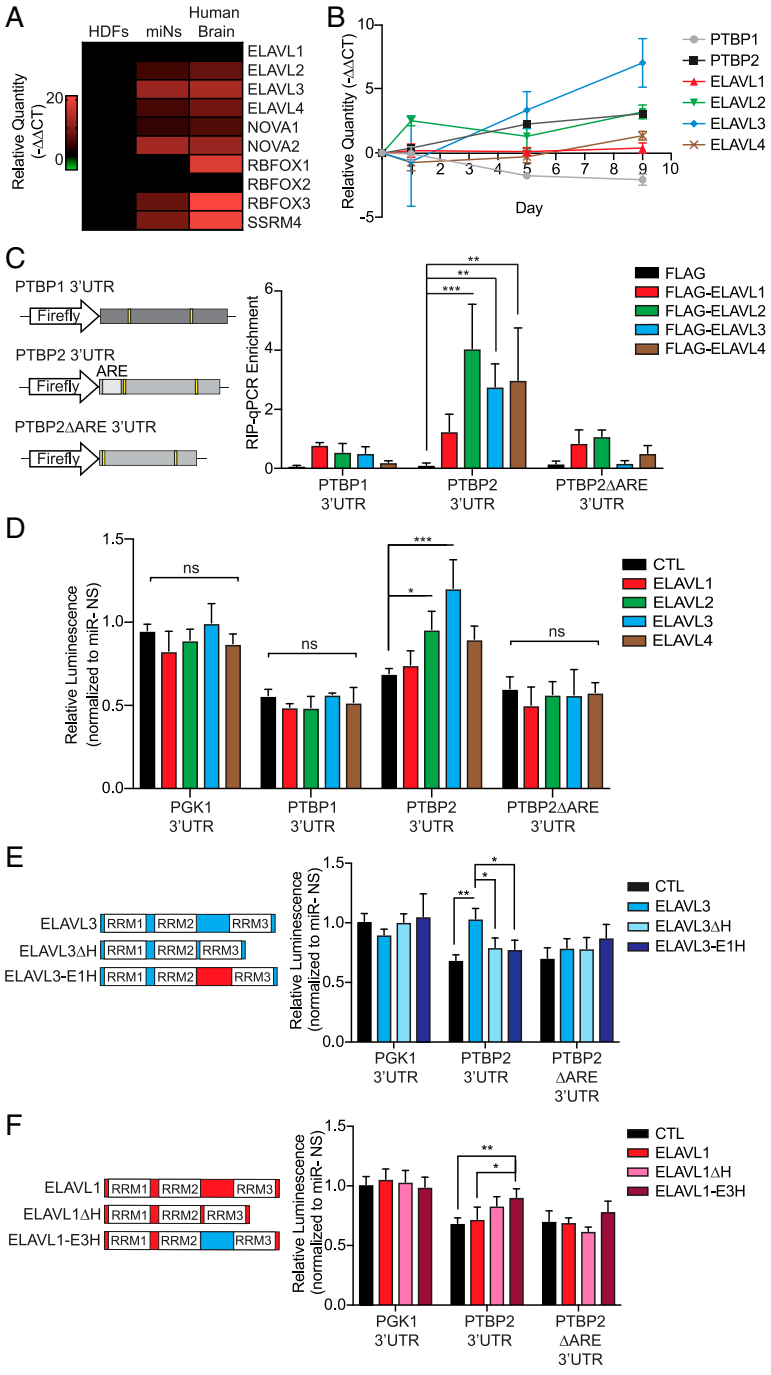

Fig. 4. MiRNA-mediated PTBP2 up-regulation requires nELAVL binding at PTBP2 3′UTR. (*A*) An expression heatmap of neuronal-enriched RBPs determined by qPCR in starting HAFs, day 30 miNs, and human brain RNA. Data from HDFs and day 30 miNs are from three independent experiments. (*B*) Time course qPCR analysis of PTB and ELAVL transcripts during neuronal reprogramming. Data are represented in ± SEM from three independent experiments for each timepoint. (*C*) (*Left*) A diagram of luciferase constructs containing different PTB 3′UTRs: PTBP1 3′UTR and PTBP2 3′UTR with and without the AU-rich element (ARE) (PTBP2ΔARE) used for RIP and luciferase assays. (*Right*) RIP of individual FLAG-tagged ELAVLs 48 h after transfection. Enrichment is normalized to input, determined by qPCR for PTBP1 or PTBP2 3′UTR. Data are represented in mean ± SEM from three independent experiments. Two-way ANOVA was performed (from left, PTBP2 3′UTR ***P = 0.0001, **P = 0.0086, 0.0042). (*D*) Luciferase assays with the addition of individual ELAVLs with luciferase constructs containing control PGK1, PTBP1, PTBP2, or PTBP2ΔARE 3′UTR. Luminescence was measured 48 h after the transfection and normalized miR-9/9*-124 to miR-NS control of each condition. Data are represented in mean ± SEM from at least three independent experiments. Two-way ANOVA was performed (*P = 0.0312, ***P = 0.0001). (*E*) (*Left*) A schematic diagram of ELAVL3 hinge (H) mutants. (*Right*) Luciferase assays with the addition of wild-type ELAVL3 or ELAVL3 hinge mutants (ELAVL3ΔH: ELAVL3 hinge deletion; ELAVL3-E1H: ELAVL3 with ELAVL1 hinge). Luminescence was measured 48 h after transfection and normalized miR-9/9*-124 to miR-NS control of each condition. Data are represented in mean ± SEM from at least four independent experiments. Two-way ANOVA was performed (from left **P = 0.0020, *P = 0.0435, *P = 0.0286). (*F*) (*Left*) A schematic diagram of ELAVL1 hinge mutants. (*Right*) Luciferase assays with the addition of wild-type ELAVL1 or ELAVL1 hinge mutants (ELAVL1ΔH: ELAVL1 hinge deletion; ELAVL1-E3H: ELAVL1 with ELAVL3 hinge). Luminescence was measured 48 h after transfection and normalized miR-9/9*-124 to miR-NS control of each condition. Data represented in mean ± SEM from at least four independent experiments. Two-way ANOVA was performed (**P = 0.0069, *P = 0.0260). ns, not significant.

program. Examples of some of these identified targets in HNs that are also validated in qPCR include *PTBP2*, *MAP2*, *SEMA6A*, *SCN1A*, and *KALRN* (Fig. 6 *D*–*F*). Together, our data support the notion that miR-124–mediated up-regulation of neuronal genes is not unique to PTBP2 in reprogramming context but applicable to other neuronal genes in actual human neurons.

MiR-124 and nELAVL Interaction for Other Neuronal Transcripts. Using existing nELAVL HITS-CLIP of the human brain (43), we performed a comparative analysis with our HNs dataset to examine whether these up-regulated neuronal transcripts are likely targets of nELAVLs. First, by overlapping 1) up-regulated neuronal DEGs bound by AGO HITS-CLIPs (Fig. 1), 2) DEGs responsive to miR-124 TuD and *ELAVL3* shRNA in HNs (Fig. 6), and 3) genes bound by nELAVLs in the human brain (43), we identified 77 genes including *PTBP2*, *MAP2*, *SLC4A8*, *KALRN*, *BCL7A*, and *SCN1A* enriched for neuronal biological terms generally involved in synaptic processes (Fig. 6*G* and *SI Appendix*, Fig. S9 and Table S4). Based on these comparisons, similar to what we observed in miNs, miR-124 and ELAVL3 appear to collectively up-regulate a set of neuronal genes that are likely critical for neuronal function in primary HNs.

Neuronal Properties Affected by miR-124 and nELAVLs. As our AGO HITS-CLIP and miR-124 KD data in miNs indicate that neuronal genes are preferentially targeted as cells acquire the neuronal fate (Figs. 1 and 2), we examined the global transcriptome changes of our CTL and KD human neurons with LONGO analysis to assess

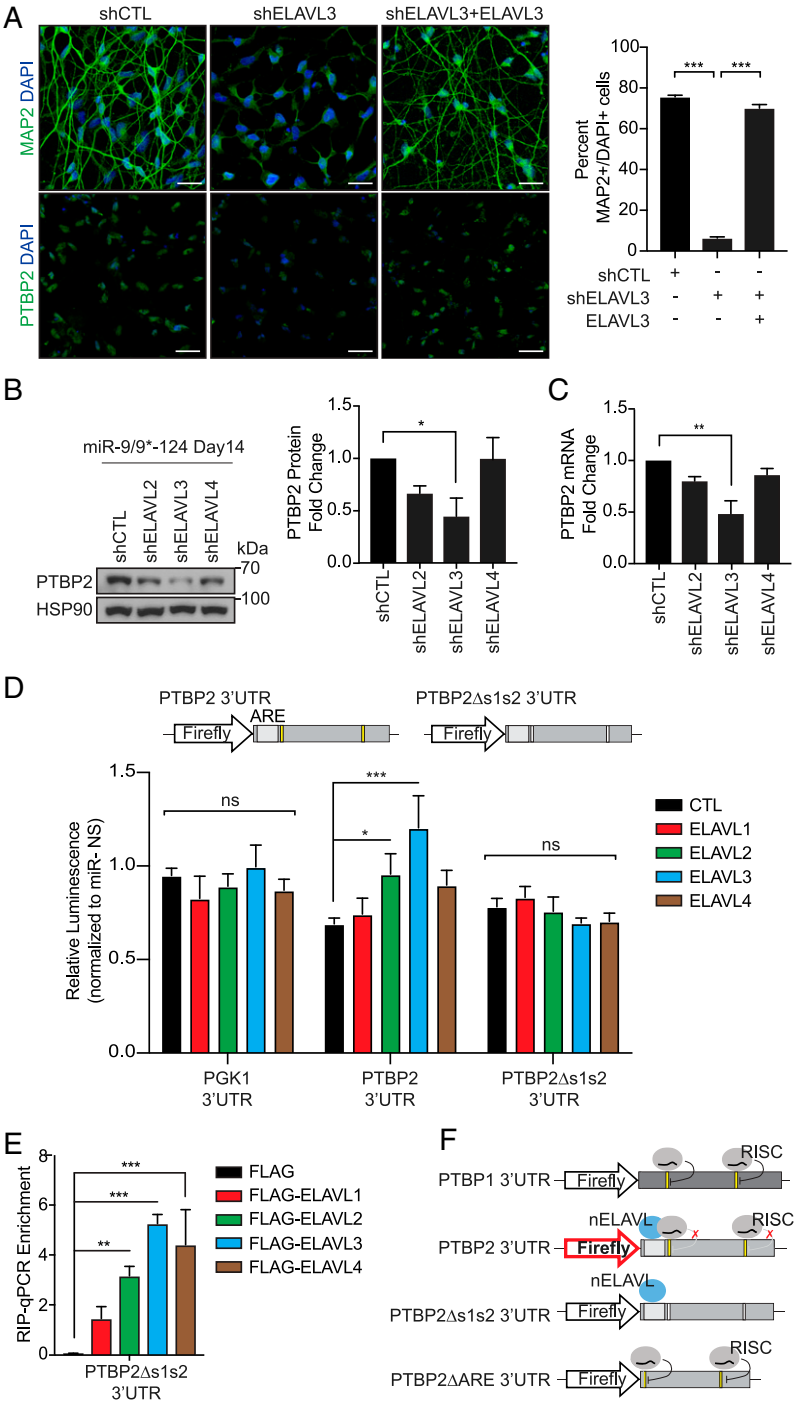

Fig. 5. PTBP2 up-regulation requires the synergism of nELAVL and miR-124. (*A*) (*Left*) Day 30 miNs with shRNA KD against CTL, ELAVL3, and ELAVL3 with ELAVL3 cDNA rescue. Cells were immunostained for MAP2 and PTBP2. (Scale bar, 50 μm.) (*Right*) Quantification of the percentage of MAP2-positive cells over the total number of DAPI-positive cells with two or more neurites (*Left*). Data represented in mean ± SEM from three separate fields of view. One-way ANOVA test was performed (from left, $***P < 0.0001$, $***P < 0.0001$). shCTL, n = MAP2 803/1060; shELAVL3, n = MAP2 67/1052; shELAVL3 + ELAVL3, n = MAP2 431/617. (*B*) (*Left*) Immunoblot analysis of PTBP2 in day 14 miNs with KD against CTL, ELAVL2, ELAVL3, and ELAVL4. (*Right*) Quantification of the PTBP2 band intensity as a relative fold change compared to shCTL normalized to HSP90 from four independent experiments. Data are represented in mean ± SEM. Two-tailed unpaired t test was performed ($*P = 0.0189$). (*C*) The relative quantity of PTBP2 transcript upon individual nELAVL KD compared to CTL at day 14 miNs determined by qPCR. Data are represented by mean ± SEM from three independent experiments. Two-tailed unpaired t test was performed ($**P = 0.002$). (*D*) (*Top*) A diagram of luciferase constructs containing PTBP2 3′UTR with or without miR-124 sites (PTBP2Δs1s2). (*Bottom*) Luciferase assays with the addition of individual ELAVLs in PGK1 control, PTBP2, or PTBP2Δs1s2 3′UTR. Luminescence was measured 48 h after transfection and normalized miR-9/9*-124 to miR-NS control of each condition. Data are represented by mean ± SEM from at least three independent experiments. Two-way ANOVA was performed ($*P = 0.0312$, $***P = 0.0001$). (*E*) RIP of individual FLAG-tagged ELAVLs in PTBP2Δs1s2 3′UTR 48 h after transfection. Enrichment normalized to input was determined through qPCR against PTBP2 3′UTR. Data are represented by mean ± SEM from three independent experiments. Two-way ANOVA was performed (from left, PTBP2Δs1s2 3′UTR $**P = 0.0018$, $***P = 0.0001$, $***P = 0.0001$). (*F*) A schematic summary of nELAVL and RISC activities on PTB 3′UTRs. ns, not significant.

changes in long gene expression, a measure of neuronal identity and maturation (46–50). Overall, KD of miR-124 and ELAVL3 (green) in HNs resulted in reduced long gene expression compared to CTL (red), suggesting that both players are likely essential for the neuronal program (Fig. 7*A*).

As a number of identified neuronal genes targeted by AGO-miR-124 and ELAVL3 in HNs are implicated in neuronal function and morphology such as *SCN1A*, *SLC4A8*, *ANK3*, and *MAP2*, reflective of reduced overall long gene expression (Fig. 7*A* and *SI Appendix*, Fig. S9*A* and Table S4), we examined a few neuronal properties in CTL and KD HNs. We first performed electrophysiology and found KD HNs exhibited reduced inward sodium current compared to CTL HNs (Fig. 7*B* and *SI Appendix*, Fig. S8*C*) which we reasoned to be attributed to a number of down-regulated channel genes in KD HNs. However, other electrical properties such as resting membrane potential and action potential firing appear similar between CTL and KD neurons (*SI Appendix*, Fig. S8 *D* and *E*). In addition, as we observed reduced neurite complexity in our KD compared to CTL HNs, we sought to measure features such as average neurite length and average number of neurite branches between the two conditions. Overall, we found that KD HNs not only have shorter average neurite length per cell but also fewer branches per cell compared to CTL (Fig. 7 *C* and *D*). Interestingly, similar results were also observed upon loss of miR-124 in human induced pluripotent stem cells-derived neurons (26).

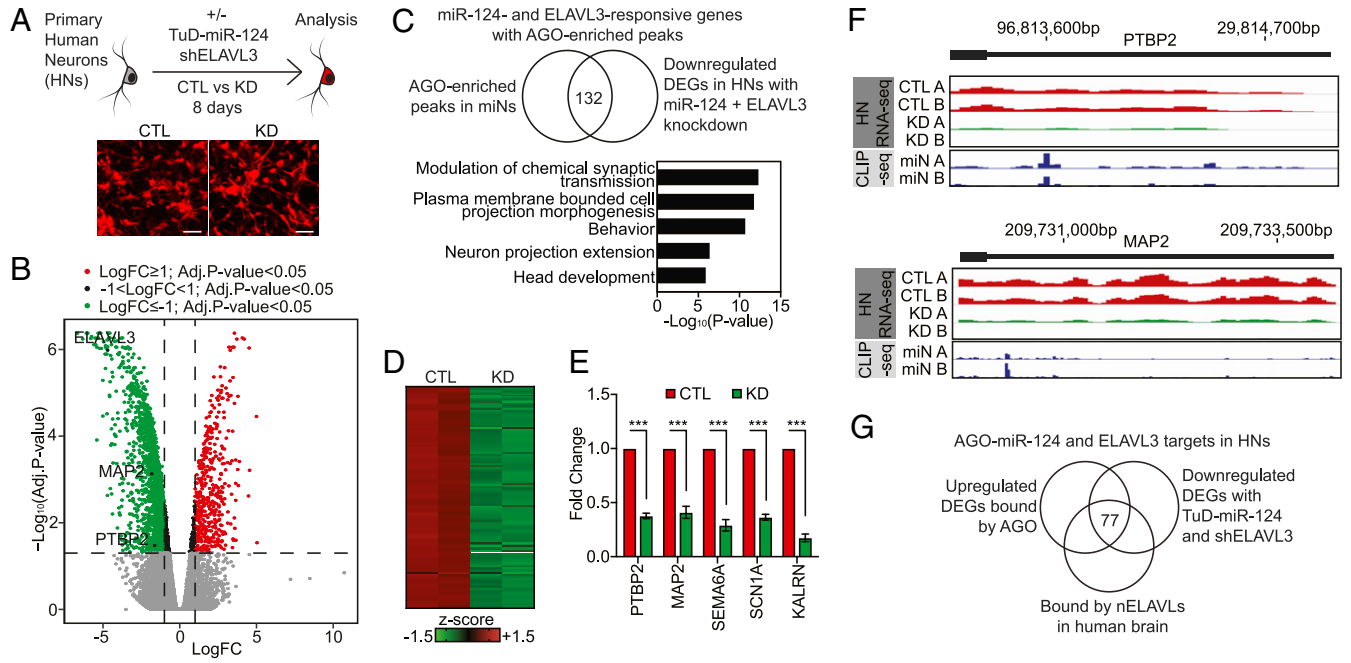

Fig. 6. MiRNA-mediated up-regulation of neuronal genes in primary human neurons. (*A*) (*Top*) A schematic diagram of the experimental procedure using primary HNs. (*Bottom*) Images of HNs marked by TurboRFP reporter in the miR-NS or miR-124 TuD. (Scale bar, 75 μm.) (*B*) A volcano plot of DEGs between CTL and KD conditions with TuD-miR-124 and shELAVL3 treatment. A selection of down-regulated genes is highlighted (ELAVL3, MAP2, and PTBP2). Red dots, HN mRNA expression; Log2FC ≥ 1, adj.*P* value < 0.05. Green dots, HN mRNA expression; Log2FC ≤ −1, adj.*P* value < 0.05. (*C*) (*Top*) By overlapping down-regulated DEGs in *A* to previously identified up-regulated AGO-enriched targets (Fig. 1), 132 genes were identified to harbor AGO peaks in miNs and are down-regulated with miR-124 and ELAVL3 KD in HNs. (*Bottom*) Top biological GO terms associated with the 132 genes. (*D*) A heatmap of the 132 genes identified in *B* from RNA-seq comparing KD and CTL HNs. (*E*) RT-qPCR validation of a select number of the identified down-regulated genes in HNs (*C*). Data are represented in ± SEM from three independent experiments. Two-tailed unpaired *t* test was performed (all, ***$P < 0.001$). (*F*) Track views of HN RNA-seq (*Top*) and miNs AGO HITS-CLIP (*Bottom*) for gene examples showing reduced expression upon KD of miR-124 and ELAVL3 in HNs (over CTL) and AGO-enriched peaks at the 3′UTR. (*G*) A Venn diagram of AGO-miR-124 targets in HNs overlapped with nELAVL-bound targets in the human brain.

Reduced expression of long genes in primary HNs with both miR-124 and ELAVL3 knocked down suggests that long gene expression is a transcriptomic phenotype reflective of altered neuronal features observed and measured in HNs. To independently validate the correlation between long gene expression and neuronal maturity, we also treated primary rat neurons with Topotecan (TOPO), an inhibitor of Topoisomerase I known to reduce long gene expression in neurons (47, 51, 52). Primary rat neurons treated with TOPO (blue) were found to display a reduction in long gene expression when compared to the control condition (dimethyl sulfoxide [DMSO], red) (Fig. 7 *E* and *F*) while the TOPO-treated cells still maintained the expression of other neuronal markers such as *Map2*, *Actl6b*, *Rbfox3*, and *Dcx* (Fig. 7*G*). To further assess the consequences of reduced long gene expression in neurons, we measured electrophysiological properties using a microelectrode array (MEA). TOPO-treated rat neurons exhibited altered electrophysiological properties compared to DMSO control, including reduced mean firing rate, mean burst frequency, and number of spikes per burst (Fig. 7*H*), demonstrating that long gene expression is a transcriptomic feature related to the functional maturity of neurons. Therefore, our results support the notion that miR-124, in synergy with ELAVL3, promote neuronal maturity by positively regulating their target genes, as evidenced by their effect on long gene expression in human neurons (Fig. 7*I*). Based on PTBP2, we delineated a mechanism on how miR-124 and ELAVL3 can promote the expression of their targets (Fig. 7*I*) and we anticipate that some of the additional identified long genes important for neuronal differentiation and function are likely up-regulated in a similar manner.

Discussion

In the present study, we uncovered the role of miR-124 in the up-regulation of genes associated with neuronal differentiation and function during the neuronal reprogramming of human fibroblasts. The use of AGO HITS-CLIP followed by miRNA–mRNA in silico prediction and experimental validation provided insights into the function of miRNAs in addition to their canonical repressor role of downstream target genes. Because of the prediction steps involved in the AGO HITS-CLIP approach, future studies using other high-throughput approaches such as cross-linking and sequencing of hybrids (CLASH) (53, 54) or photoactivatable ribonucleoside-enhanced crosslinking and immunoprecipitation (PAR-CLIP) (55) that identifies chimera sequences between miRNA–mRNA interactions would provide more direct identification of other non-canonical targets and base pairing of miRNAs.

Of the bound AGO transcripts are bona fida miR-124 target genes in which the 3′UTRs can be repressed in a nonneuronal context but reversed upon neuronal induction. By examining the mutually exclusive regulation of *PTBP1* and *PTBP2*, we reveal how miR-124 plays a bifunctional role depending on the sequence composition of the 3′UTR, the availability of neuronal ELAVLs, and the interaction with AGOs to mediate the switching of PTB homolog expression during the neuronal conversion of HDFs (Fig. 7*I*). Although we focus specifically on the interplay between miR-124 and ELAVL3 for PTBP2 up-regulation, future studies should also examine whether a similar mechanism is used to promote other identified neuronal transcripts or whether other RBPs can also synergize with AGO for such target gene regulation. For example, FXR1, anRBP, has been shown in previous studies

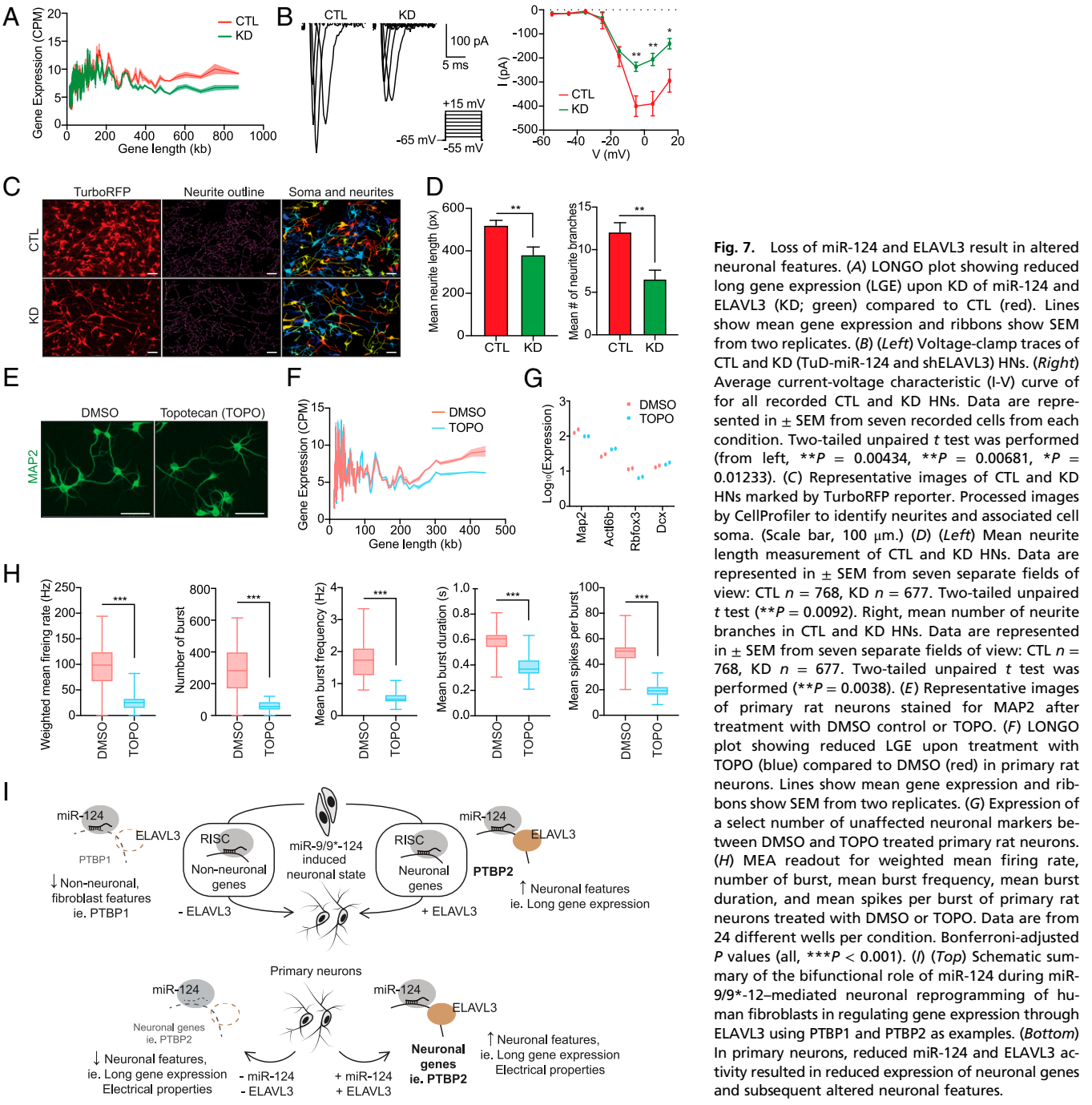

Fig. 7. Loss of miR-124 and ELAVL3 result in altered neuronal features. (*A*) LONGO plot showing reduced long gene expression (LGE) upon KD of miR-124 and ELAVL3 (KD; green) compared to CTL (red). Lines show mean gene expression and ribbons show SEM from two replicates. (*B*) (*Left*) Voltage-clamp traces of CTL and KD (TuD-miR-124 and shELAVL3) HNs. (*Right*) Average current-voltage characteristic (I-V) curve of for all recorded CTL and KD HNs. Data are represented in ± SEM from seven recorded cells from each condition. Two-tailed unpaired *t* test was performed (from left, $^{**}P = 0.00434$, $^{**}P = 0.00681$, $^{*}P = 0.01233$). (*C*) Representative images of CTL and KD HNs marked by TurboRFP reporter. Processed images by CellProfiler to identify neurites and associated cell soma. (Scale bar, 100 μm.) (*D*) (*Left*) Mean neurite length measurement of CTL and KD HNs. Data are represented in ± SEM from seven separate fields of view: CTL $n = 768$, KD $n = 677$. Two-tailed unpaired *t* test ($^{**}P = 0.0092$). Right, mean number of neurite branches in CTL and KD HNs. Data are represented in ± SEM from seven separate fields of view: CTL $n = 768$, KD $n = 677$. Two-tailed unpaired *t* test was performed ($^{**}P = 0.0038$). (*E*) Representative images of primary rat neurons stained for MAP2 after treatment with DMSO control or TOPO. (*F*) LONGO plot showing reduced LGE upon treatment with TOPO (blue) compared to DMSO (red) in primary rat neurons. Lines show mean gene expression and ribbons show SEM from two replicates. (*G*) Expression of a select number of unaffected neuronal markers between DMSO and TOPO treated primary rat neurons. (*H*) MEA readout for weighted mean firing rate, number of burst, mean burst frequency, mean burst duration, and mean spikes per burst of primary rat neurons treated with DMSO or TOPO. Data are from 24 different wells per condition. Bonferroni-adjusted *P* values (all, $^{***}P < 0.001$). (*I*) (*Top*) Schematic summary of the bifunctional role of miR-124 during miR-9/9*-12–mediated neuronal reprogramming of human fibroblasts in regulating gene expression through ELAVL3 using PTBP1 and PTBP2 as examples. (*Bottom*) In primary neurons, reduced miR-124 and ELAVL3 activity resulted in reduced expression of neuronal genes and subsequent altered neuronal features.

to interact with AGO to facilitate gene expression in nonneuronal cells (17–19).

The selective role of ELAVL3 and not ubiquitous ELAVL1 in mediating PTBP2 induction in neurons highlights the functional specificity of ELAVL family members in neurons. Like ELAVL3, ELAVL1 binds AREs and has been shown to interact with RISC components (18, 56). Although different studies reveal opposing consequences of RISC and ELAVL family interaction on target genes, downstream functional output of AGO-ELAVL likely depends on not only the concurrent availability of RBPs and target transcript but also the 3′UTR sequence. Our results define the functional specificity inherent in ELAVL3 that cannot be replaced by ELAVL1, especially for regulating PTBP2 expression with miR-124 in neurons. We found that the specificity is, at least in part, driven by the hinge region inferred by the region-swapping experiments between ELAVL1 and ELAVL3. As there is no known AU-rich motif recognition unique to each ELAVL family member, it is likely that interactors associating with the hinge region may be regulating ELAVL specificity and targeting (45, 57).

To investigate whether the synergism of miR-124 and nELAVLs for transcript stabilization and activation can be generalized to other neuronal transcripts beyond *PTBP2* outside the conversion system, we also knocked down miR-124 and ELAVL3 in primary human neurons. Our results indicate that several neuronal transcripts are induced by miR-124 and ELAVL3 that are critical for neuronal program. Furthermore, by examining an existing nELAVL HITS-CLIP dataset in the human brain (43), we uncovered that miR-124- and nELAVL-mediated up-regulation of target transcripts may not

be a unique occurrence to *PTBP2* but likely an overlooked mechanism that maintains gene expression in neurons. Interestingly, as we identified numerous neuronal genes to be targets of miR-124, such as *MAP2*, *CAMK1D*, and *SEMA6A*, we argue that miR-124 may be critical for enhancing the overall neuronal program as measured by the reduced sodium current and neurite length and branches through its regulation on long genes. By chemically inhibiting long gene expression in rat neurons, mimicking the transcriptomic phenotype observed in human neurons with reduced miR-124 and ELAVL3 activity, we observed a variety of altered electrical properties. This finding also indicates that miR-9/9*-124 is highly neurogenic as these miRNAs not only allow for the conversion of human fibroblasts into neurons (1, 12) but also enhanced the expression of neuronal markers, such as *MAP2*, when overexpressed during neuronal differentiation of human pluripotent stem cell–derived neurons (58, 59). Although further tests are required to see whether all the identified transcripts targeted by both miR-124 and nELAVLs share the same mechanism as *PTBP2*, our loss-of-function results from both reprogramming and primary human neuron systems and its effect on other neuronal genes support to the general role of miR-124 as a positive regulator of select target genes in neurons. Future experiments taking a closer look at RNA structure, motif proximity with RBPs, and additional interacting proteins will provide further mechanistic insights to how a single miRNA can simultaneously repress and activate different transcripts in a cell context–dependent manner.

Materials and Methods

Cell Culture. Primary human fibroblasts used in this study include 22-y-old female (GM02171, National Institute of General Medical Sciences [NIGMS] Coriell Institute for Medical Research), 36-y-old female (AG05838, National Institute of Aging [NIA] Coriell Institute for Medical Research), 2-y-old male (AG07095, NIA Coriell Institute for Medical Research), and neonatal fibroblasts (ScienCell, 2310). MiR-9/9*-124–mediated reprogramming is initiated as previously described (60). E18 rat cortex (BrainBits, FSDECX1M) and primary human neurons from 18 to 22 wk of gestation were obtained commercially (ScienCell, 1520) with gender of the source undisclosed. Additional cell culture details and methods regarding immunostaining, qPCR, and immunoblot on reprogrammed cells and neurons can be found in *SI Appendix, Supplementary Materials and Methods*.

Sequencing. AGO HITS-CLIP was performed on cells after 2 wk into reprogramming of miR-NS or miR-9/9*-124–expressing neonatal fibroblasts (ScienCell, 2310) at day 14 and day 21. Approximately, 1×10^7 cells were crosslinked with ultraviolet (UV) light, harvested, lysed, and processed according to Moore et al., 2014 (61). Additional details regarding HITS-CLIP preparation and processing can be found in *SI Appendix, Supplementary Materials and Methods*. MiRNA TuD RNA-seq was performed on day 21 cells expressing miR-9/9*-124 + TuD-miR-NS and miR-9/9*-124 + TuD-miR-124 as well as HNs treated with TuDs for 8 d using TRIzol Reagent (Invitrogen, 15596026) in combination with RNeasy micro kit (Qiagen, 74004). For E18 rat cortical neurons, RNA was collected using TRIzol Reagent (Invitrogen, 15596026) in combination with RNeasy micro kit (Qiagen, 74004). For Human Clariom D Array (Affymetrix), total RNA was extracted from day 14 cells expressing miR-NS, miR-9/9*-124 + shCTL, and miR-9/9*-124 + shPTBP2 using TRIzol Reagent in combination with RNeasy mini kit (Qiagen, 74104). Sequencing and microarray datasets are accessible through GSE161241 and GSE120918.

Electrophysiology. Whole-cell patch-clamp recordings were performed as previously described (62). Briefly, HNs (ScienCell, 1521) were recorded within 8 to 10 d after TuD and shRNA transduction. For MEA, E18 rat cortical neurons (BrainBits, FSDECX1M) were treated with either Topotecan (Sigma-Aldrich, T2705) or DMSO control for 1 wk before recording electrophysiological activity using a Maestro MEA plate reader (Axion Biosystems). Details on electrophysiology can be found in *SI Appendix, Supplementary Materials and Methods*.

Data Availability. Sequencing data have been deposited in Gene Expression Omnibus (GSE161241 and GSE120918).

ACKNOWLEDGMENTS. We thank the Genome Technology Access Center (GTAC) at Washington University for the sequencing service and support and flow Cytometry Core at Washington University for equipment use. We thank P. Gontarz for the bioinformatics help in the initial analysis of AGO HITS-CLIP, D. Annamalai and A. H. Kim for the help with TuD designs, M. Victor for the help with electrophysiology, C. Karch for the help with MEA, and K. Cates and L. Capano for the helpful suggestions with the manuscript. Y.L.L. is supported by the LIFENAD Fellowship. M.J.M. was supported by the Interface of Psychology, Neuroscience and Genetics (IPNG) fellowship (T32GM081739; Barch, PI). This study was supported through awards and funds to A.S.Y. by the Andrew B. and Virginia C. Craig Faculty Fellowship endowment, NIH Director's Innovator Award (DP2NS083372), Presidential Early Career Award for Scientists and Engineers, and NIH (RF1AG056296 and R01NS107488).

1. D. G. Abernathy *et al.*, MicroRNAs induce a permissive chromatin environment that enables neuronal subtype-specific reprogramming of adult human fibroblasts. *Cell Stem Cell* **21**, 332–348.e9 (2017).
2. K. Cates *et al.*, Deconstructing stepwise fate conversion of human fibroblasts to neurons by MicroRNAs. *Cell Stem Cell* **28**, 127–140.e9 (2021).
3. Y.-L. Lu, A. S. Yoo, Mechanistic insights into microRNA-induced neuronal reprogramming of human adult fibroblasts. *Front. Neurosci.* **12**, 522 (2018).
4. S. W. Lee, Y. M. Oh, Y.-L. Lu, W. K. Kim, A. S. Yoo, MicroRNAs overcome cell fate barrier by reducing EZH2-controlled REST stability during neuronal conversion of human adult fibroblasts. *Dev. Cell* **46**, 73–84.e7 (2018).
5. C. J. Schoenherr, D. J. Anderson, The neuron-restrictive silencer factor (NRSF): A coordinate repressor of multiple neuron-specific genes. *Science* **267**, 1360–1363 (1995).
6. N. Ballas, C. Grunseich, D. D. Lu, J. C. Speh, G. Mandel, REST and its corepressors mediate plasticity of neuronal gene chromatin throughout neurogenesis. *Cell* **121**, 645–657 (2005).
7. J. Lessard *et al.*, An essential switch in subunit composition of a chromatin remodeling complex during neural development. *Neuron* **55**, 201–215 (2007).
8. B. T. Staahl *et al.*, Kinetic analysis of npBAF to nBAF switching reveals exchange of SS18 with CREST and integration with neural developmental pathways. *J. Neurosci.* **33**, 10348–10361 (2013).
9. K. Tsutsui, K. Tsutsui, K. Sano, A. Kikuchi, A. Tokunaga, Involvement of DNA topoisomerase IIbeta in neuronal differentiation. *J. Biol. Chem.* **276**, 5769–5778 (2001).
10. M. Watanabe, K. Tsutsui, K. Tsutsui, Y. Inoue, Differential expressions of the topoisomerase II alpha and II beta mRNAs in developing rat brain. *Neurosci. Res.* **19**, 51–57 (1994).
11. A. S. Yoo, B. T. Staahl, L. Chen, G. R. Crabtree, MicroRNA-mediated switching of chromatin-remodelling complexes in neural development. *Nature* **460**, 642–646 (2009).
12. A. S. Yoo *et al.*, MicroRNA-mediated conversion of human fibroblasts to neurons. *Nature* **476**, 228–231 (2011).
13. E. V. Makeyev, J. Zhang, M. A. Carrasco, T. Maniatis, The MicroRNA miR-124 promotes neuronal differentiation by triggering brain-specific alternative pre-mRNA splicing. *Mol. Cell* **27**, 435–448 (2007).
14. A. N. Packer, Y. Xing, S. Q. Harper, L. Jones, B. L. Davidson, The bifunctional microRNA miR-9/miR-9* regulates REST and CoREST and is downregulated in Huntington's disease. *J. Neurosci.* **28**, 14341–14346 (2008).
15. J. Visvanathan, S. Lee, B. Lee, J. W. Lee, S.-K. Lee, The microRNA miR-124 antagonizes the anti-neural REST/SCP1 pathway during embryonic CNS development. *Genes Dev.* **21**, 744–749 (2007).
16. M. B. Victor *et al.*, Generation of human striatal neurons by microRNA-dependent direct conversion of fibroblasts. *Neuron* **84**, 311–323 (2014).
17. S. S. Truesdell *et al.*, MicroRNA-mediated mRNA translation activation in quiescent cells and oocytes involves recruitment of a nuclear microRNP. *Sci. Rep.* **2**, 842 (2012).
18. S. Vasudevan, J. A. Steitz, AU-rich-element-mediated upregulation of translation by FXR1 and Argonaute 2. *Cell* **128**, 1105–1118 (2007).
19. S. Vasudevan, Y. Tong, J. A. Steitz, Switching from repression to activation: microRNAs can up-regulate translation. *Science* **318**, 1931–1934 (2007).
20. J. Lu, H. Ji, H. Tang, Z. Xu, microRNA-124a suppresses PHF19 over-expression, EZH2 hyper-activation, and aberrant cell proliferation in human glioma. *Biochem. Biophys. Res. Commun.* **503**, 1610–1617 (2018).
21. W. H. Neo *et al.*, MicroRNA miR-124 controls the choice between neuronal and astrocyte differentiation by fine-tuning Ezh2 expression. *J. Biol. Chem.* **289**, 20788–20801 (2014).
22. S. Zhou *et al.*, MiR-9 inhibits Schwann cell migration by targeting Cthrc1 following sciatic nerve injury. *J. Cell Sci.* **127**, 967–976 (2014).
23. M. Rehmsmeier, P. Steffen, M. Hochsmann, R. Giegerich, Fast and effective prediction of microRNA/target duplexes. *RNA* **10**, 1507–1517 (2004).
24. T. Haraguchi, Y. Ozaki, H. Iba, Vectors expressing efficient RNA decoys achieve the long-term suppression of specific microRNA activity in mammalian cells. *Nucleic Acids Res.* **37**, e43 (2009).
25. R. O. Bak, A. K. Hollensen, M. N. Primo, C. D. Sørensen, J. G. Mikkelsen, Potent microRNA suppression by RNA pol II-transcribed 'tough decoy' inhibitors. *RNA* **19**, 280–293 (2013).
26. L. K. Kutsche *et al.*, Combined experimental and system-level analyses reveal the complex regulatory network of miR-124 during human neurogenesis. *Cell Syst.* **7**, 438–452.e8 (2018).
27. Y. Xue *et al.*, Sequential regulatory loops as key gatekeepers for neuronal reprogramming in human cells. *Nat. Neurosci.* **19**, 807–815 (2016).

28. P. L. Boutz *et al*., A post-transcriptional regulatory switch in polypyrimidine tract-binding proteins reprograms alternative splicing in developing neurons. *Genes Dev.* **21**, 1636–1652 (2007).
29. Q. Li *et al*., The splicing regulator PTBP2 controls a program of embryonic splicing required for neuronal maturation. *eLife* **3**, e01201 (2014).
30. D. D. Licatalosi *et al*., Ptbp2 represses adult-specific splicing to regulate the generation of neuronal precursors in the embryonic brain. *Genes Dev.* **26**, 1626–1642 (2012).
31. J. K. Vuong *et al*., PTBP1 and PTBP2 serve both specific and redundant functions in neuronal pre-mRNA splicing. *Cell Rep.* **17**, 2766–2775 (2016).
32. S. Zheng *et al*., PSD-95 is post-transcriptionally repressed during early neural development by PTBP1 and PTBP2. *Nat. Neurosci.* **15**, 381–388, S1 (2012).
33. T. Glisovic, J. L. Bachorik, J. Yong, G. Dreyfuss, RNA-binding proteins and post-transcriptional gene regulation. *FEBS Lett.* **582**, 1977–1986 (2008).
34. V. Iadevaia, A. P. Gerber, Combinatorial control of mRNA fates by RNA-binding proteins and non-coding RNAs. *Biomolecules* **5**, 2207–2222 (2015).
35. P. Jiang, H. Coller, Functional interactions between microRNAs and RNA binding proteins. *MicroRNA* **1**, 70–79 (2012).
36. M. Plass, S. H. Rasmussen, A. Krogh, Highly accessible AU-rich regions in 3′ untranslated regions are hotspots for binding of regulatory factors. *PLoS Comput. Biol.* **13**, e1005460 (2017).
37. K. B. Cook, H. Kazan, K. Zuberi, Q. Morris, T. R. Hughes, RBPDB: A database of RNA-binding specificities. *Nucleic Acids Res.* **39**, D301–D308 (2011).
38. I. Paz, I. Kosti, M. Ares Jr, M. Cline, Y. Mandel-Gutfreund, RBPmap: A web server for mapping binding sites of RNA-binding proteins. *Nucleic Acids Res.* **42**, W361–W367 (2014).
39. H. Yu, J. Wang, Q. Sheng, Q. Liu, Y. Shyr, beRBP: Binding estimation for human RNA-binding proteins. *Nucleic Acids Res.* **47**, e26 (2019).
40. K. Lin *et al*., Essential requirement of mammalian *Pumilio* family in embryonic development. *Mol. Biol. Cell* **29**, 2922–2932 (2018).
41. D. S. Spassov, R. Jurecic, Cloning and comparative sequence analysis of PUM1 and PUM2 genes, human members of the Pumilio family of RNA-binding proteins. *Gene* **299**, 195–204 (2002).
42. H. J. Okano, R. B. Darnell, A hierarchy of Hu RNA binding proteins in developing and adult neurons. *J. Neurosci.* **17**, 3024–3037 (1997).
43. C. Scheckel *et al*., Regulatory consequences of neuronal ELAV-like protein binding to coding and non-coding RNAs in human brain. *eLife* **5**, e10421 (2016).
44. G. Ince-Dunn *et al*., Neuronal Elav-like (Hu) proteins regulate RNA splicing and abundance to control glutamate levels and neuronal excitability. *Neuron* **75**, 1067–1080 (2012).
45. M. N. Hinman, H.-L. Zhou, A. Sharma, H. Lou, All three RNA recognition motifs and the hinge region of HuC play distinct roles in the regulation of alternative splicing. *Nucleic Acids Res.* **41**, 5049–5061 (2013).
46. H. W. Gabel *et al*., Disruption of DNA-methylation-dependent long gene repression in Rett syndrome. *Nature* **522**, 89–93 (2015).
47. I. F. King *et al*., Topoisomerases facilitate transcription of long genes linked to autism. *Nature* **501**, 58–62 (2013).
48. M. J. McCoy *et al*., LONGO: An R package for interactive gene length dependent analysis for neuronal identity. *Bioinformatics* **34**, i422–i428 (2018).
49. M. J. McCoy, A. Z. Fire, Intron and gene size expansion during nervous system evolution. *BMC Genomics* **21**, 360 (2020).
50. K. Sugino *et al*., Cell-type-specific repression by methyl-CpG-binding protein 2 is biased toward long genes. *J. Neurosci.* **34**, 12877–12883 (2014).
51. A. M. Mabb *et al*., Topoisomerase 1 regulates gene expression in neurons through cleavage complex-dependent and -independent mechanisms. *PLoS One* **11**, e0156439 (2016).
52. A. M. Mabb *et al*., Topoisomerase 1 inhibition reversibly impairs synaptic function. *Proc. Natl. Acad. Sci. U.S.A.* **111**, 17290–17295 (2014).
53. A. Helwak, G. Kudla, T. Dudnakova, D. Tollervey, Mapping the human miRNA interactome by CLASH reveals frequent noncanonical binding. *Cell* **153**, 654–665 (2013).
54. G. Kudla, S. Granneman, D. Hahn, J. D. Beggs, D. Tollervey, Cross-linking, ligation, and sequencing of hybrids reveals RNA-RNA interactions in yeast. *Proc. Natl. Acad. Sci. U.S.A.* **108**, 10010–10015 (2011).
55. S. Grosswendt *et al*., Unambiguous identification of miRNA:target site interactions by different types of ligation reactions. *Mol. Cell* **54**, 1042–1054 (2014).
56. H. H. Kim *et al*., HuR recruits let-7/RISC to repress c-Myc expression. *Genes Dev.* **23**, 1743–1748 (2009).
57. T. Fujiwara *et al*., Functional and direct interaction between the RNA binding protein HuD and active Akt1. *Nucleic Acids Res.* **40**, 1944–1953 (2012).
58. M. Ishikawa *et al*., miRNA-based rapid differentiation of purified neurons from hPSCs advancestowards quick screening for neuronal disease phenotypes in vitro. *Cells* **9**, 532 (2020).
59. A. X. Sun *et al*., Direct induction and functional maturation of forebrain GABAergic neurons from human pluripotent stem cells. *Cell Rep.* **16**, 1942–1953 (2016).
60. M. Richner, M. B. Victor, Y. Liu, D. Abernathy, A. S. Yoo, MicroRNA-based conversion of human fibroblasts into striatal medium spiny neurons. *Nat. Protoc.* **10**, 1543–1555 (2015).
61. M. J. Moore *et al*., Mapping Argonaute and conventional RNA-binding protein interactions with RNA at single-nucleotide resolution using HITS-CLIP and CIMS analysis. *Nat. Protoc.* **9**, 263–293 (2014).
62. M. B. Victor *et al*., Striatal neurons directly converted from Huntington's disease patient fibroblasts recapitulate age-associated disease phenotypes. *Nature Neurosci.* **21**, 341–352 (2018).